Electronic Supplementary Material (ESI) for Physical Chemistry Chemical Physics.

Vibronic interaction in CO_3^- photo-detachment: Jahn-Teller effects beyond structural distortion and general formalisms for vibronic Hamiltonians in trigonal symmetries

Supplementary Information

Issaka Seidu,[†,‡] Prateek Goel,[¶] Xiao-Gang Wang,[§] Bo Chen,[‖] Xue-Bin Wang,[⊥] and Tao Zeng[*,†]

†*Department of Chemistry, Carleton University, Ottawa, Ontario, K1S5B6, Canada*

‡*Department of Chemistry and Biomolecular Sciences, University of Ottawa, 10 Marie Curie, Ottawa, Ontario, K1N6N5, Canada*

¶*Department of Chemistry, University of Florida, Gainesville, Florida, 32601, United States*

§*Department of Chemistry, Queen's University, Kingston, Ontario, K7L3N6, Canada*

‖*Department of Chemistry, Pennsylvania State University, State College, Pennsylvania, 16801, United States*

⊥*Pacific Northwest National Laboratory, Richland, Washington, 99352, United States*

E-mail: toby.zeng@carleton.ca

List of Figures

List of Tables

Section S1 General formalisms of Jahn-Teller and pseudo-Jahn-Teller vibronic Hamiltonian operators in trigonal symmetries

The feasibility of organizing general formalisms of Jahn-Teller and pseudo-Jahn-Teller vibronic Hamiltonian operators in one type of axial symmetries in tables has been elaborated on in Ref. 1. Here, we skip the detailed derivations and only present the tabulated formulas for obtaining all bimodal JT and pJT Hamiltonians in all trigonal symmetries, i.e., the C_3, C_{3v}, D_3, C_{3h}, D_{3h}, and D_{3d} symmetries. Please note the isomorphism between the C_{3v} and D_3 groups, and the isomorphism between the D_{3h} and D_{3d} groups. D_{3h} is a composite of D_3 and C_{3h}. The σ_v-type symmetry elements in C_{3v} are replaced by the C_2'-type symmetry elements in D_3. The σ_h in D_{3h} is replaced by the I in D_{3d}. In D_{3h} and D_{3d}, the subscript 1 and 2 of the A-type irreducible representation (irrep) indicates being even and odd, respectively, with respect to $\hat{C}_2'$, not $\hat{\sigma}_v$. This is why we consider D_{3h} being a composite of D_3 and C_{3h}, instead of C_{3v} and C_{3h}.

A Settings of states and vibrational modes

The tabulated formalisms are for a specific setting of electronic states and vibrational coordinates. All electronic states are transformed to be eigenstates of $\hat{C}_3$. A-type states are $\hat{C}_3$-eigenstates with the eigenvalue $\chi^{C_3} = 1$. E-type states take a complex form, i.e.,

$$|\pm\rangle = \frac{1}{\sqrt{2}} \left(|X\rangle \pm i\, |Y\rangle \right), \tag{S1}$$

with $|X\rangle$ and $|Y\rangle$ being the conventional real components that transform as the unit vectors along the right-hand-rule x and y axes under the $\hat{C}_3$ rotation about the z axis. The complex

E-type states satisfy the eigenvalue equations:

$$\hat{C}_3 \left|\pm\right\rangle = e^{\mp i \frac{2\pi}{3}} \left|\pm\right\rangle . \tag{S2}$$

The so-defined complex components swap under the time-reversal operation. They are further defined so that the they swap under $\hat{\sigma}_v$ and $\hat{C}_2'$.

The a-type vibrational coordinate is represented by z. The polar coordinates ρ and ϕ are used to describe e-type vibration. They are related to the conventional cartesian e-type coordinates x and y as $x = \rho\cos\phi$ and $y = \rho\sin\phi$. Figure S1 exemplifies the cartesian components of the e-type vibrations and the real components of the E-type states in the six trigonal symmetries. **Please note that the tabulated formalisms are applicable strictly to the E-type states and E-type vibrations that orient following the same conventions in Figure S1. Specifically, $\hat{C}_3 \left|X\right\rangle = -\frac{1}{2}\left|X\right\rangle + \frac{\sqrt{3}}{2}\left|Y\right\rangle$; $\hat{C}_3 \left|X\right\rangle = -\frac{1}{2}\left|Y\right\rangle - \frac{\sqrt{3}}{2}\left|X\right\rangle$, and the similar transformations for the e components. Also, the $\left|X\right\rangle$ and e_x must be symmetric with respect to the demonstrated $\hat{C}_2'$ operation in D_3, D_{3h}, and D_{3d} symmetries, and with respect to the demonstrated $\hat{\sigma}_v$ in C_{3v} symmetry. The $\left|Y\right\rangle$ and e_y must be antisymmetric correspondingly.**

B General forms of the vibronic Hamiltonians in trigonal symmetries

JT and pJT Hamiltonian operators are usually resolved in a set of strongly interacting states in a diabatic representation. When the states are degenerate at the undistorted high symmetry configuration, their vibronic coupling gives the JT effect. When they are non-degenerate, their coupling gives the pJT effect. Since the couplings in the JT interaction are between states belonging to the same term symbol, we call this type of couplings *intra*-term couplings. Following the same logic, we call the vibronic couplings in pJT interaction *inter*-term couplings. Figure S2 exemplifies the two types of coupling using two sets of E-type

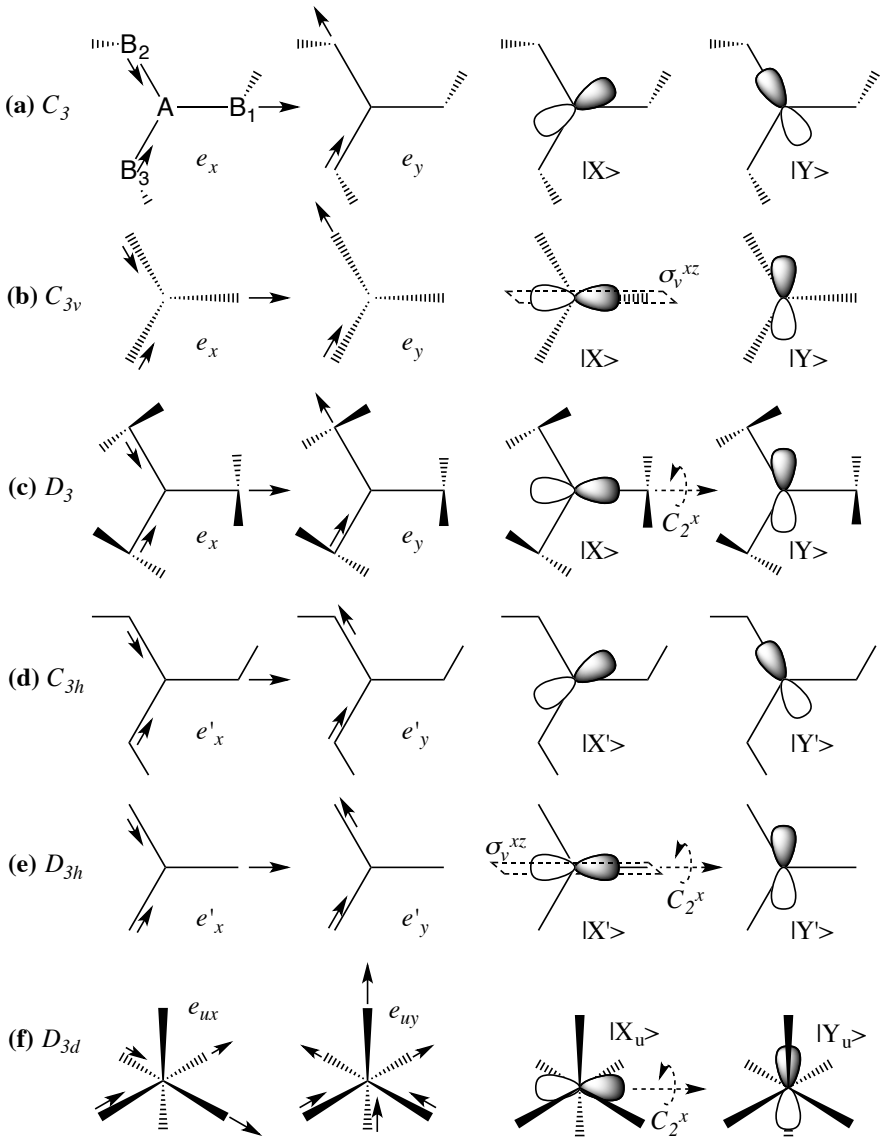

Figure S1: Examples of orientations of e and E components, on which the derivations are based. Atomic motions in the modes are represented by solid arrows. With the atom labelling in panel (a), $e_x = \sqrt{\frac{1}{6}}\,(2\Delta r_{AB_1} - \Delta r_{AB_2} - \Delta r_{AB_3})$, and $e_y = \sqrt{\frac{1}{2}}\,(\Delta r_{AB_2} - \Delta r_{AB_3})$. Similar definitions apply to the displayed e modes in the other panels.

states. Throughout this work, we use the greek letters α and β to differentiate states or modes with the same irreducible representations. Please do not mistake them for electronic spin functions.

Since there are two types of irreps in trigonal symmetries, A and E, there are two types of intra-term couplings and three types of inter-term couplings: $(A + A)$, $(E + A)$, and

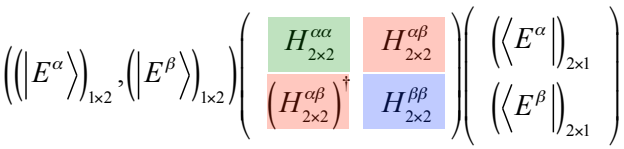

Figure S2: The matrix product form of a vibronic coupling Hamiltonian that involves two E term symbols denoted by α and β. The green and blue diagonal blocks of the H matrix give the intraterm couplings, and the red off-diagonal blocks give the interterm coupling.

$(E+E)$. These vibronic couplings have the following respective forms of Hamiltonians:

1. For $(A+A)$-type couplings, $\hat{H} = |A_\alpha\rangle \langle A_\beta| H^r_{A_\alpha A_\beta}$, with the states and the matrix element being real (denoted by the superscript r). The A-type coupling takes the same form of Hamiltonian.

2. For $(E+A)$-type couplings, $\hat{H} = (|+\rangle \langle A| + |A\rangle \langle -|) H_{+A} + hc$. hc stands for the hermitian conjugate of the explicitly written part of the Hamiltonian. H_{+A} is complex-valued. The fact that the $|+\rangle \langle A|$ and $|A\rangle \langle -|$ dyads share the same matrix element is determined by the time-reversal symmetry of the Hamiltonian, in the absence of an external magnetic field. This reason also applies to all parenthesized pairs of dyads in the Hamiltonians below. It will not be repeated.

3. For $(E+E)$-type couplings,
   $\hat{H} = (|+_\alpha\rangle \langle +_\beta| + |-_\beta\rangle \langle -_\alpha|) H_{+_\alpha +_\beta} + (|+_\alpha\rangle \langle -_\beta| + |+_\beta\rangle \langle -_\alpha|) H_{+_\alpha -_\beta} + hc$. The matrix elements are complex-valued.

4. For E-type couplings, $\hat{H} = (|+\rangle \langle +| + |-\rangle \langle -|) H^r_{++} + |+\rangle \langle -| H_{+-} + |-\rangle \langle +| H^*_{+-}$. Again, the r superscript indicates that H_{++} is real-valued.

Only independent Hamiltonian matrix elements are kept in those Hamiltonian operator expressions. The construction of a JT or pJT Hamiltonian is to find the symmetry-adapted expansion formulas of the matrix elements in vibrational coordinates of the relevant vibrational modes.

C Symmetry requirements on the matrix elements

The only requirement on the Hamiltonian operators is that they must be invariant with respect to all symmetry operations of the relevant point groups. Actually, they only need to be invariant with respect to representation operations. The representative operations are: $\hat{C}_3$ for all the six point groups; one of the three $\hat{\sigma}_v$s ($\hat{C}'_2$s) in C_{3v} (D_3, D_{3h}, and D_{3d}); $\hat{\sigma}_h$ in C_{3h} and D_{3h}; $\hat{I}$ in D_{3d}.

Since all the bras and kets in the Hamiltonians are $\hat{C}_3$-eigenstates, to have the Hamiltonians to be $\hat{C}_3$-invariant, their matrix elements must be $\hat{C}_3$-eigenfunctions, with the eigenvalues that are reciprocal of the products of the $\hat{C}_3$-eigenvalues of the corresponding bras and kets. These $\hat{C}_3$-eigenvalues (χ^{C_3}s) of all the independent matrix elements are summarized in Table S1. In C_{3v} symmetry, $\hat{\sigma}_v$ swaps $|+\rangle$ and $|-\rangle$ and hence imposes constraints on the matrix elements, that they need to satisfy $\hat{\sigma}_v H_{ij} = H^*_{ij}$ or $\hat{\sigma}_v H_{ij} = -H^*_{ij}$. The matrix elements do not in general need to be $\hat{\sigma}_v$-eigenfunctions, but their real and imaginary parts do need to be. The required $\hat{\sigma}_v$-eigenvalues of the matrix elements' real and imaginary parts, $(\chi^{\sigma_v}_{Re}, \chi^{\sigma_v}_{Im})$s, are summarized in Table S1. Note that $\chi^{\sigma_v}_{Im} = 0$ indicates that the matrix element is real-valued. In D_3 symmetry, the role of $\hat{\sigma}_v$ is replaced by $\hat{C}'_2$. All the other arguments still apply. The same set of $\left(\chi^{C'_2}_{Re}, \chi^{C'_2}_{Im}\right)$s are also given in the table.

Table S1: The eigenvalues of symmetry operators of the independent elements in trigonal vibronic Hamiltonian matrices. The $\hat{\sigma}_v$- and $\hat{C}_2$-eigenvalues are given for the real and imaginary parts of the matrix elements separately. The heading $(E+E)$ means the matrix elements underneath are relevant to the $(E+E)$ problems, etc. k and l stand for the 1 and 2 subscripts when σ_v or C'_2 are relevant. p and q stand for the $'$ and $''$ superscripts when σ_h is relevant. Although p and q are placed as superscripts, they also stand for possible g and u subscripts when I is relevant.

	$(A+A)/A$	$(E+A)$
ij: $\chi^{C_3}, (\chi^{\sigma_v,C'_2}_{Re}, \chi^{\sigma_v,C'_2}_{Im}), \chi^{\sigma_h,I}$	$A^p_k A^q_l$: $1, ((-1)^{\delta_{kl}+1}, 0), (-1)^{\delta_{pq}+1}$	$+^p A^q_k$: $e^{\frac{i2\pi}{3}}, ((-1)^{\delta_{k2}}, (-1)^{\delta_{k1}}), (-1)^{\delta_{pq}+1}$
	$(E+E)$	E
ij: $\chi^{C_3}, (\chi^{\sigma_v,C'_2}_{Re}, \chi^{\sigma_v,C'_2}_{Im}), \chi^{\sigma_h,I}$	$+^p_\alpha +^q_\beta$: $1, (1,-1), (-1)^{\delta_{pq}+1}$ $+^p_\alpha -^q_\beta$: $e^{-i\frac{2\pi}{3}}, (1,-1), (-1)^{\delta_{pq}+1}$	$++$: $1, (1,0), 1$ $+-$: $e^{-i\frac{2\pi}{3}}, (1,-1), 1$

In C_{3h}, the bras and kets are $\hat{\sigma}_h$-eigenstates. Correspondingly, the matrix elements need to be $\hat{\sigma}_h$-eigenstates with eigenvalues equal to the products of those of the associated bras and kets. The required $\hat{\sigma}_h$-eigenstates are also summarized in Table S1. To summarize, for a JT or pJT Hamiltonian operator in C_3 symmetry, its matrix elements need to have the specific χ^{C_3}s; in C_{3v} symmetry, χ^{C_3}s and $(\chi^{\sigma_v}_{Re}, \chi^{\sigma_v}_{Im})$s; in D_3 symmetry, χ^{C_3}s and $\left(\chi^{C'_2}_{Re}, \chi^{C'_2}_{Im}\right)$s; in C_{3h} symmetry, χ^{C_3}s and χ^{σ_h}s; in the composite D_{3h} symmetry, χ^{C_3}s, $\left(\chi^{C'_2}_{Re}, \chi^{C'_2}_{Im}\right)$s, and χ^{σ_h}s; in D_{3d} symmetry, χ^{C_3}s, $\left(\chi^{C'_2}_{Re}, \chi^{C'_2}_{Im}\right)$s, and χ^{I}s. In short, the invariance requirement of the JT and pJT Hamiltonian operators has been translated into the symmetry-eigenvalues of the independent matrix elements. The construction of a JT or pJT Hamiltonian is hence to find the expansions of the matrix elements in relevant vibrational coordinates, and the expansions need to be eigenfunctions of the symmetry operators with the appropriate eigenvalues. We call those expansions symmetry-adapted expansions.

D Symmetry-adapted expansions

The symmetry-adapted expansions of the different combinations of vibrational coordinates can be obtained using projection operators. The procedure is detailed in Ref. 1 and is not repeated here. We provide the symmetry-adapted expansion formulas for bimodal JT and pJT Hamiltonians, i.e., the problems that involve two sets of vibrational modes such as $E \otimes (e + a)$, $(E + A) \otimes (e + e)$, etc. Unimodal expansions are special cases of the bimodal expansions with one set of coordinates being set to be zero. Hamiltonian operators involving more than two modes can be approximated as combinations of bimodal Hamiltonians. For instance, the $(E' + E') \otimes (e'' + a'_1 + a'_2)$ problem in D_{3h} symmetry can be approximated as the combinations of the $(E' + E') \otimes (e'' + a'_1)$, $(E' + E') \otimes (e'' + a'_2)$, and $(E' + E') \otimes (a'_1 + a'_2)$ problems.

The bimodal expansions with $\chi^{C_3} = 1$ and $e^{i\frac{2\pi}{3}}$ are given in Tables S2 and S3, respectively. Einstein's convention of summing over duplicate indices is applied in those expansions and throughout the whole work. a and b are the expansion coefficients. The I, m, and n are

summation indices. Whenever they appear in the absolute value signs, they take all integer values. Otherwise, they only take nonzero integer values. The superscripts r and i of the a and b coefficients indicate that the coefficients arise from the real and imaginary parts, respectively, of the coefficients without the superscripts. a^r, a^i, b^r, and b^i are all real. We do not provide the expansions with $\chi^{C_3} = e^{-i\frac{2\pi}{3}}$, although this χ^{C_3} appears in Table S1. This is because they are just the complex conjugates of the expansions with $\chi^{C_3} = e^{i\frac{2\pi}{3}}$.

We call the expansions in Tables S2 and S3 root formulas. They are expansions for the JT and pJT Hamiltonians in the lowest C_3 symmetry (root). Expansions for Hamiltonians in the higher trigonal symmetries are obtained by imposing constraints onto them, so that the resultant expansions also bear eigenvalues of the symmetry operators in addition to $\hat{C}_3$.

Table S2: Expansion formulas for $\hat{C}_3$-eigenfunctions of the bimodal vibrational coordinates with eigenvalue 1.

Modes	Expansion formulas
$(a+a)$	$a^r_{I_1,I_2} z_\alpha^{I_1} z_\beta^{I_2} + i a^i_{I_3,I_4} z_\alpha^{I_3} z_\beta^{I_4}$
$(e+a)$	$a^{3m}_{I,2K} z^I \rho^{\lvert 3m\rvert+2K} e^{i3m\phi} = \rho^{\lvert 3m\rvert+2K}[a^{r,3m}_{I_1,2K} z^{I_1}\cos(3m\phi) - a^{i,3m}_{I_2,2K} z^{I_2}\sin(3m\phi)$ $+i\left(a^{r,3m}_{I_1,2K} z^{I_1}\sin(3m\phi) + a^{i,3m}_{I_2,2K} z^{I_2}\cos(3m\phi)\right)]$
$(e+e)$	$a^{m,3n}_{2K_1,2K_2}\rho_\alpha^{\lvert m\rvert+2K_1}\rho_\beta^{\lvert 3n-m\rvert+2K_2} e^{i(m\phi_\alpha+(3n-m)\phi_\beta)} = \rho_\alpha^{\lvert m\rvert+2K_1}\rho_\beta^{\lvert 3n-m\rvert+2K_2}$ $\left[(a^{r,m,3n}_{2K_1,2K_2}\cos(m\phi_\alpha+(3n-m)\phi_\beta) - a^{i,m,3n}_{2K_1,2K_2}\sin(m\phi_\alpha+(3n-m)\phi_\beta)\right.$ $\left.+i(a^{r,m,3n}_{2K_1,2K_2}\sin(m\phi_\alpha+(3n-m)\phi_\beta) + a^{i,m,3n}_{2K_1,2K_2}\cos(m\phi_\alpha+(3n-m)\phi_\beta))\right]$

Table S3: Expansion formulas for $\hat{C}_3$-eigenfunctions of the bimodal vibrational coordinates with eigenvalue $e^{i\frac{2\pi}{3}}$.

Modes	Expansion formulas
$(a+a)$	not applicable (na)
$(e+a)$	$b^{3n-1}_{I,2K} z^I \rho^{\lvert 3n-1\rvert+2K} e^{i(3n-1)\phi} = \rho^{\lvert 3n-1\rvert+2K}\left[b^{r,3n-1}_{I_1,2K} z^{I_1}\cos((3n-1)\phi) - b^{i,3n-1}_{I_2,2K} z^{I_2}\sin((3n-1)\phi)\right.$ $\left.+i\left(b^{r,3n-1}_{I_1,2K} z^{I_1}\sin((3n-1)\phi) + b^{i,3n-1}_{I_2,2K} z^{I_2}\cos((3n-1)\phi)\right)\right]$
$(e+e)$	$b^{m,3n-1}_{2K_1,2K_2}\rho_\alpha^{\lvert m\rvert+2K_1}\rho_\beta^{\lvert 3n-1-m\rvert+2K_2} e^{i(m\phi_\alpha+(3n-1-m)\phi_\beta)} = \rho_\alpha^{\lvert m\rvert+2K_1}\rho_\beta^{\lvert 3n-1-m\rvert+2K_2}$ $\left[b^{r,m,3n-1}_{2K_1,2K_2}\cos(m\phi_\alpha+(3n-1-m)\phi_\beta) - b^{i,m,3n-1}_{2K_1,2K_2}\sin(m\phi_\alpha+(3n-1-m)\phi_\beta)\right.$ $\left.+i\left(b^{r,m,3n-1}_{2K_1,2K_2}\sin(m\phi_\alpha+(3n-1-m)\phi_\beta) + b^{i,m,3n-1}_{2K_1,2K_2}\cos(m\phi_\alpha+(3n-1-m)\phi_\beta)\right)\right]$

The constraints that give the appropriate $\left(\chi_{Re}^{\sigma_v,C_2'}, \chi_{Im}^{\sigma_v,C_2'}\right)$s for JT and pJT Hamiltonians in C_{3v} and D_3 symmetries are summarized in Tables S4 and S5. The constraints that

give the appropriate χ^{σ_h}s for JT and pJT Hamiltonians in C_{3h} symmetry are summarized in Tables S6 and S7. Please note that the constraints in Tables S5 and S7 are also applicable for the matrix elements with $\chi^{C_3} = e^{-i\frac{2\pi}{3}}$. For JT and pJT Hamiltonians in D_{3h} symmetry, we simply need to combine the constraints from all these tables, whichever applicable. Again, the JT and pJT Hamiltonians in D_{3d} symmetry share the same expansion formulas with those in D_{3h}, but with $'$ and $''$ being correspondingly replaced by the subscripts g and u.

Table S4: Constraints on expansions in Table S2 to give the appropriate $\chi_{Re}^{\sigma_v,C_2'}$ and $\chi_{Im}^{\sigma_v,C_2'}$. When $\chi_{Im}^{\sigma_v,C_2'} = 0$, only the real part of the corresponding entry in Table S2 should be considered.

Modes	$1,(1,0)$	$1,(-1,0)$	$1,(1,-1)$
(a_1+a_1)	nr[†]	na	na
(a_1+a_2)[‡]	I_2 even[¶]	I_2 odd	I_2 even, I_4 odd
(a_2+a_2)	I_1, I_2 ee or oo[§]	I_1, I_2 eo or oe[£]	I_1, I_2 ee or oo, I_3, I_4 eo or oe
$(e+a_1)$	cos nz[#]	sin nz	a^r nz
$(e+a_2)$	I_1 even, I_2 odd	I_1 odd, I_2 even	I_1 even, I_2 odd
$(e+e)$	cos nz	sin nz	a^r nz

[†] "nr" means "no restriction". [‡] For two modes whose irreps only differ in subscripts, α-subscripted coordinates in Table S2 are for the first (a_1 here) and β- for the second (a_2 here) mode. [¶] I_2 needs to be even. [§] I_1 and I_2 need to be both even or both odd. [£] When I_1 is even, I_2 must be odd, and vice versa. [#] Only the terms associated with cosine factors are nonzero.

Table S5: Constraints on expansions in Table S3 to give the appropriate $\chi_{Re}^{\sigma_v,C_2'}$ and $\chi_{Im}^{\sigma_v,C_2'}$.

Modes	$e^{i\frac{2\pi}{3}},(1,-1)$	$e^{i\frac{2\pi}{3}},(-1,1)$
$(e+a_1)$	b^r nz	b^i nz
$(e+a_2)$	I_1 even, I_2 odd	I_1 odd, I_2 even
$(e+e)$	b^r nz	b^i nz

Table S6: Constraints on expansions in Table S2 to give the appropriate $\left(\chi^{C_3}=1,\chi^{\sigma_h,I}\right)$. The modes here are given for σ_h. The $'$ and $''$ can be correspondingly replaced by the g and u subscripts for the D_{3d} symmetry.

Vibrational Modes	$(1,1)$	$(1,-1)$
$(a'+a')$	nr	na
$(a'+a'')^{\dagger}$	I_2, I_4 even	I_2, I_4 odd
$(a''+a'')$	I_1, I_2 ee or oo I_3, I_4 ee or oo	I_1, I_2 eo or oe I_3, I_4 eo or oe
$(e'+a')$	nr	na
$(e''+a')$	$3m$ even	$3m$ odd
$(e'+a'')$	I even	I odd
$(e''+a'')$	$3m, I$ ee or oo	$3m, I$ eo or oe
$(e'+e')$	nr	na
$(e''+e')$	m even	m odd
$(e''+e'')$	$3n$ even	$3n$ odd

† For two modes whose irreps only differ in subscripts, α-subscripted coordinates in Table S2 are for the first (a' here) and β- for the second (a'' here) mode. This rule applies in all constraints tables.

Table S7: Constraints on expansions in Table S3 to give the appropriate $\left(\chi^{C_3}=e^{i\frac{2\pi}{3}},\chi^{\sigma_h,I}\right)$. The modes here are given for σ_h. The $'$ and $''$ can be correspondingly replaced by the g and u subscripts for the D_{3d} symmetry.

Vibrational Modes	$(e^{i\frac{2\pi}{3}},1)$	$(e^{i\frac{2\pi}{3}},-1)$
$(e'+a')$	nr	na
$(e''+a')$	$3n$ odd	$3n$ even
$(e'+a'')$	I even	I odd
$(e''+a'')$	$3n$ even,I odd $3n$ odd, I even	$3n$ even,I even $3n$ odd, I odd
$(e'+e')$	nr	na
$(e''+e')$	m even	m odd
$(e''+e'')$	$3n$ odd	$3n$ even

Section S2 Expansion formulas of the JT and pJT Hamiltonians for the two lowest-lying E-type triplet states of CO_3.

This work is about simulating the lowest energy triplet band in the negative ion photoelectron spectrum of CO_3^-, and the two lowest triplet states of CO_3 have the $^3E''$ and the $^3E'$ term symbols. There are six vibrational modes in CO_3, and they transform as a_1', a_2'', e', and e' irreps. These symmetry-adapted internal vibrations are shown in Figure S3, with their normalized coordinates being labelled as s_1 to s_6. The total vibronic problem thus contains $E'' \otimes (a_1' + a_2'' + 2e')$ and $E' \otimes (a_1' + a_2'' + 2e')$ intra-term problems, and an $(E'' + E') \otimes (a_1' + a_2'' + 2e')$ inter-term problem. We use these JT and pJT problems as examples to demonstrate how to get the vibronic Hamiltonian expansions using the tables above. For each of these problems, we single out the totally symmetric a_1 stretching, which is JT- and pJT-inactive, from the rest. The diabatic potentials of the four component states of the two E-type terms depend on the a_1 stretching, and these dependences are expressed as Morse potential functions, i.e.,

$$V_{+''+''}(s_1) = V_{-''-''}(s_1) = E_{E'',min} + D_{E''}(1 - e^{-\alpha_{E''}\left(s_1 - s_{1,min}^{E''}\right)})^2, \tag{S3}$$

and a similar form for the potentials of the $^3E'$ state. $s_{1,min}^{E''}$ is the coordinate corresponding to the minimum of the potential ($E_{E'',min}$) along the stretching. $D_{E''}$ and $\alpha_{E''}$ are the conventional Morse parameters that determine the depth and width of the potential well.

The calculated and fitted Morse potential energy curve of the $^3E''$ energy along s_1 is shown in Figure S3 as an example. A perfect agreement is seen. Since only the calculated energies around the minimum are used for the fitting, the fitted $D_{E''} = 17.28$ eV shall be viewed as a fitting parameter that gives small fitting errors at the this range of s_1, instead of the true dissociation energy. The potential energy curves of the other states along s_1 look

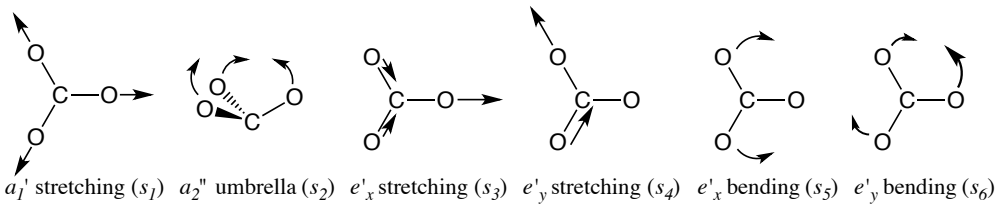

Figure S3: The six symmetry-adapted internal vibrations of CO_3. In the e'_x stretching and the e'_y bending vibration, the motions along the long arrows are twice of those along the short arrows.

similar and display similarly perfect agreements. They are hence not shown.

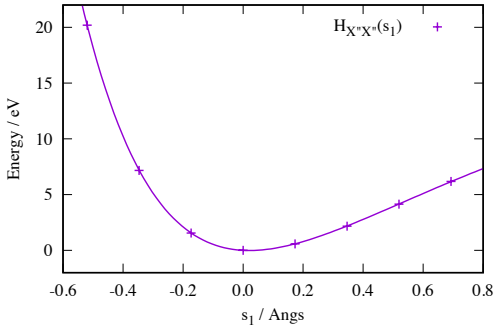

Figure S4: The calculated and the fitted Morse potential energy curve of the $^3E''$ energy along s_1.

The leftover $(a''_2 + 2e')$ vibrations are decomposed to bimodal combinations of two $(a''_2 + e')$ parts and one $(e' + e')$ part. For the $E'' \otimes (a''_2 + e')$ intra-term problem, there are two independent matrix elements in Table S1, $H_{+''+''}$ and $H_{+''-''}$, whose symmetry eigenvalues are $(1, (1, 0), 1)$ and $(1, (1, -1), 1)$, respectively. The root expansion of $H_{+''+''}$ is taken from the $(e + a)$ row in Table S2:

$$\begin{aligned} H_{++} &= \rho^{|3m|+2K} \left[a^{r,3m}_{I_1,2K} z^{I_1} \cos 3m\phi - a^{i,3m}_{I_2,2K} z^{I_2} \sin 3m\phi \right. \\ &\quad \left. + i a^{r,3m}_{I_1,2K} z^{I_1} \sin 3m\phi + i a^{r,3m}_{I_2,2K} z^{I_2} \cos 3m\phi \right] . \end{aligned} \tag{S4}$$

In the following, we look up the constraints on this expansion in Table S4, where the $(e + a_2)$-$(1, (1, 0))$ entry reads I_1 can only take even integers, while I_2 odd only. The last constraint is in the $(e' + a'')$-$(1, 1)$ entry in Table S6, which reads all Is have to be even. Combining

the last two constraints, only the terms with even I_1 remain in the expansion in Eq. S4:

$$H_{+''+''} = a^{r,3m}_{2I_1,2K} z^{2I_1} \rho^{|3m|+2K} e^{i3m\phi}. \tag{S5}$$

The $\chi^{C_2'}_{Im} = 0$ determines that only the real part shall be kept. Therefore,

$$\begin{aligned} H_{+''+''} &= a^{r,3m}_{2I_1,2K} z^{2I_1} \rho^{|3m|+2K} \cos 3m\phi \\ &= a^{r,3m}_{2I_1,2K} z^{2I_1} \rho^{3m+2K} \cos 3m\phi. \end{aligned} \tag{S6}$$

Please note that the absolute value symbols of $3m$ are removed in the second row to remove the duplicate terms. Correspondingly, m now only takes nonnegative integers. Using the coordinate symbols in Figure S3, z is replaced by s_2 and ρ and ϕ are calculated using s_3 and s_4 for the e' stretching, whereas using s_5 and s_6 fro the e' bending. These substitutions of coordinates shall be kept in mind and will not be repeated below.

The root expansion of $H_{+''-''}$ is obtained by taking the complex conjugate of the $(e+a)$ row's entry in Table S3:

$$\begin{aligned} H_{+-} = \rho^{|3n-1|+2K} \big[& b^{r,3n-1}_{I_1,2K} z^{I_1} \cos(3n-1)\phi - b^{i,3n-1}_{I_2,2K} z^{I_2} \sin(3n-1)\phi \\ & -ib^{r,3n-1}_{I_1,2K} z^{I_1} \sin(3n-1)\phi - ib^{i,3n-1}_{I_2,2K} z^{I_2} \cos(3n-1)\phi \big]. \end{aligned} \tag{S7}$$

Then we apply the constraint of "I_1 even, I_2 odd" in the $(e+a_2)$-$\left(e^{i\frac{2\pi}{3}}, (1,-1)\right)$ entry in Table S5 and the "I even" constraint in the $(e'+a'') - \left(e^{i\frac{2\pi}{3}}, 1\right)$ entry in Table S7. Together, the constraints mean only the terms with even I_1 shall remain:

$$H_{+''-''} = b^{r,3n-1}_{2I_1,2K} z^{2I_1} \rho^{|3n-1|+2K} e^{-i(3n-1)\phi}. \tag{S8}$$

$H_{+'+'}$ and $H_{+'-'}$ share the same expansion formulas as $H_{+''+''}$ and $H_{+''-''}$, respectively, but with different sets of expansion coefficients. This is because the product of the σ_h-parities

are both even in the two intra-term couplings.

Back-transforming the complex E components to the real components (i.e., the inverse of the transformation in Eq. S1), we have the following real-valued expansions for the Hamiltonian matrix elements:

$$\begin{aligned}
\frac{H_{X''X''} + H_{Y''Y''}}{2} &= H_{+''+''} = a^{r,3m}_{2I_1,2K} z^{2I_1} \rho^{3m+2K} \cos 3m\phi; \\
\frac{H_{X''X''} - H_{Y''Y''}}{2} &= Re\left(H_{+''-''}\right) = b^{r,3n-1}_{2I_1,2K} z^{2I_1} \rho^{|3n-1|+2K} \cos\left(3n-1\right)\phi; \\
H_{X''Y''} &= -Im\left(H_{+''-''}\right) = b^{r,3n-1}_{2I_1,2K} z^{2I_1} \rho^{|3n-1|+2K} \sin\left(3n-1\right)\phi. \qquad \text{(S9)}
\end{aligned}$$

Please note that the b^r coefficients are shared by two expansions in this real representation of the ${}^3E''$ state. Again, the same expansion formulas apply for the real ${}^3E'$ components, but with different sets of coefficients. This sharing of expansion formulas between the E'' and E' intra-term problems will not be repeated below.

The root formulas for the $E'' \otimes (e' + e')$ are given in the $(e + e)$ rows in Tables S2 and S3 (recalling taking the complex conjugate for the expansion in Table S3):

$$\begin{aligned}
H_{++} &= \rho_\alpha^{|m|+2K_1} \rho_\beta^{|3n-m|+2K_2} \left[a^{r,m,3n}_{2K_1,2K_2} \cos\left(m\phi_\alpha + (3n-m)\,\phi_\beta\right) - a^{i,m,3n}_{2K_1,2K_2} \sin\left(m\phi_\alpha + (3n-m)\,\phi_\beta\right) \right. \\
&\quad \left. + i a^{r,m,3n}_{2K_1,2K_2} \sin\left(m\phi_\alpha + (3n-m)\,\phi_\beta\right) + i a^{i,m,3n}_{2K_1,2K_2} \cos\left(m\phi_\alpha + (3n-m)\,\phi_\beta\right) \right]; \qquad \text{(S10)} \\
H_{+-} &= \rho_\alpha^{|m|+2K_1} \rho_\beta^{|3n-1-m|+2K_2} \left[b^{r,m,3n-1}_{2K_1,2K_2} \cos\left(m\phi_\alpha + (3n-1-m)\,\phi_\beta\right) \right. \\
&\quad - b^{i,m,3n-1}_{2K_1,2K_2} \sin\left(m\phi_\alpha + (3n-1-m)\,\phi_\beta\right) - i b^{r,m,3n-1}_{2K_1,2K_2} \sin\left(m\phi_\alpha + (3n-1-m)\,\phi_\beta\right). \\
&\quad \left. - i b^{i,m,3n-1}_{2K_1,2K_2} \cos\left(m\phi_\alpha + (3n-1-m)\,\phi_\beta\right) \right]. \qquad \text{(S11)}
\end{aligned}$$

The $(e + e)$-$(1, (1, 0))$ entry in Table S4 is "cos nz" and the $(e' + e')$-$(1, 1)$ entry in Table S6 is "nr". So, only the cosine, real-valued terms remain in the H_{++} expansion above:

$$H_{+''+''} = a^{r,m,3n}_{2K_1,2K_2} \rho_\alpha^{|m|+2K_1} \rho_\beta^{|3n-m|+2K_2} \cos\left(m\phi_\alpha + (3n-m)\,\phi_\beta\right). \qquad \text{(S12)}$$

The $(e+e)$-$\left(e^{i\frac{2\pi}{3}},(1,-1)\right)$ entry in Table S5 is "b^r nz" and the $(e'+e')$-$\left(e^{i\frac{2\pi}{3}},1\right)$ entry in Table S7 is "nr". Only the terms with b^r remain in the H_{+-} root expansion above:

$$H_{+''-''} = b^{r,m,3n-1}_{2K_1,2K_2}\rho_\alpha^{|m|+2K_1}\rho_\beta^{|3n-1-m|+2K_2}e^{-i\left(m\phi_\alpha+(3n-1-m)\phi_\beta\right)}. \quad \text{(S13)}$$

Similar to the results in Eq. S9, the transformation to the real E'' components gives

$$\begin{aligned}
\frac{H_{X''X''}+H_{Y''Y''}}{2} &= H_{+''+''} = a^{r,m,3n}_{2K_1,2K_2}\rho_\alpha^{|m|+2K_1}\rho_\beta^{|3n-m|+2K_2}\cos\left(m\phi_\alpha+(3n-m)\phi_\beta\right);\\
\frac{H_{X''X''}-H_{Y''Y''}}{2} &= Re\left(H_{+''-''}\right)\\
&= b^{r,m,3n-1}_{2K_1,2K_2}\rho_\alpha^{|m|+2K_1}\rho_\beta^{|3n-1-m|+2K_2}\cos\left(m\phi_\alpha+(3n-1-m)\phi_\beta\right);\\
H_{X''Y''} &= -Im\left(H_{+''-''}\right)\\
&= b^{r,m,3n-1}_{2K_1,2K_2}\rho_\alpha^{|m|+2K_1}\rho_\beta^{|3n-1-m|+2K_2}\sin\left(m\phi_\alpha+(3n-1-m)\phi_\beta\right). \quad \text{(S14)}
\end{aligned}$$

Now the $(E''+E')\otimes(e'+a_2'')$ expansions. In Table S1, there are two independent matrix elements for this inter-term coupling, $H_{+''+'}$ and $H_{+''-'}$, with the symmetry eigenvalues $(1,(1,-1),-1)$ and $\left(e^{-i\frac{2\pi}{3}},(1,-1),-1\right)$. The $(e+a)$ root formulas in Eqs. S4 and S7 still apply to the two matrix elements, given the same χ^{C_3}s. Applying the constraints of "I_1 even, I_2 odd" (the $(e+a_2)$-$(1,(1,-1))$ entry in Table S4) and "I odd" (the $(e'+a'')$-$(1,-1)$ entry in Table S6), only the odd I_2 terms remain in Eq. S4:

$$\begin{aligned}
H_{+''+'} &= ia^{i,3m}_{2I_2+1,2K}z^{2I_2+1}\rho^{|3m|+2K}e^{i3m\phi}\\
&= a^{s,3m}_{2I_2+1,2K}z^{2I_2+1}\rho^{3m+2K}\sin 3m\phi + ia^{c,3m}_{2I_2+1,2K}z^{2I_2+1}\rho^{3m+2K}\cos 3m\phi. \quad \text{(S15)}
\end{aligned}$$

In the second row, a^s and a^c are real coefficients for the sine and cosine terms. The absolute value symbols of $3m$ has been dropped to remove duplicate terms in the final expansion, and m now only takes nonnegative integers. Applying the constraints of "I_1 even, I_2 odd" (the $(e+a_2)$-$\left(e^{i\frac{2\pi}{3}},(1,-1)\right)$ entry in Table S5) and "I odd" (the $(e'+a'')$-$\left(e^{i\frac{2\pi}{3}},-1\right)$ entry

in Table S7), only the odd I_2 terms remain in Eq. S7:

$$H_{+''-'} = -ib^{i,3n-1}_{2I_2+1,2K} z^{2I_2+1} \rho^{|3n-1|+2K} e^{-i(3n-1)\phi}. \quad \text{(S16)}$$

Back-transforming to the real $^3E''$ and real $^3E'$ components, we have

$$\begin{aligned}
\frac{H_{X''X'} + H_{Y''Y'}}{2} &= Re\left(H_{+''+'}\right) = a^{s,3m}_{2I_2+1,2K} z^{2I_2+1} \rho^{3m+2K} \sin 3m\phi \\
\frac{H_{X''X'} - H_{Y''Y'}}{2} &= Re\left(H_{+''-'}\right) = -b^{i,3n-1}_{2I_2+1,2K} z^{2I_2+1} \rho^{|3n-1|+2K} \sin\left(3n-1\right)\phi; \\
\frac{H_{X''Y'} + H_{Y''X'}}{2} &= -Im\left(H_{+''-'}\right) = b^{i,3n-1}_{2I_2+1} z^{2I_2+1} \rho^{|3n-1|+2K} \cos\left(3n-1\right)\phi; \\
\frac{H_{X''Y'} - H_{Y''X'}}{2} &= Im\left(H_{+''+'}\right) = a^{c,3m}_{2I_2+1,2K} z^{2I_2+1} \rho^{3m+2K} \cos 3m\phi. \quad \text{(S17)}
\end{aligned}$$

Please note that in actual calculations, our $|X''\rangle$ ($|Y''\rangle$) is symmetric (antisymmetric) with respect to $\hat{\sigma}_v$, instead of $\hat{C}'_2$. This is because we did the CO_3 calculations before standardizing the formalisms. With the non-standard $|X''\rangle$ and $|Y''\rangle$,

$$\begin{aligned}
\frac{H_{X''X'} + H_{Y''Y'}}{2} &= a^{c,3m}_{2I_2+1,2K} z^{2I_2+1} \rho^{3m+2K} \cos 3m\phi; \\
\frac{H_{X''X'} - H_{Y''Y'}}{2} &= -b^{i,3n-1}_{2I_2+1} z^{2I_2+1} \rho^{|3n-1|+2K} \cos\left(3n-1\right)\phi; \\
\frac{H_{X''Y'} + H_{Y''X'}}{2} &= -b^{i,3n-1}_{2I_2+1,2K} z^{2I_2+1} \rho^{|3n-1|+2K} \sin\left(3n-1\right)\phi; \\
\frac{H_{X''Y'} - H_{Y''X'}}{2} &= -a^{s,3m}_{2I_2+1,2K} z^{2I_2+1} \rho^{3m+2K} \sin 3m\phi. \quad \text{(S18)}
\end{aligned}$$

These four are the expansion formulas that we use for fitting the model and simulating the NIPE spectrum.

There is no $(E'' + E') \otimes (e' + e')$ coupling because of the odd parities of the matrix elements and the even parities of the vibrational coordinates. Following the same path in finding the expansion formulas in the Tables, we end up with "na".

Eqs. S9, S14, and S18 give all expansion formulas we need in simulating the CO_3^- NIPE spectrum in this work. They are complete (not missing any terms), concise (redundancy-

free), and convenient to obtain. It takes only a few minutes to get them by using those tables. Certainly, it will be as convenient to obtain expansion formulas for any bimodal JT and pJT Hamiltonians in trigonal symmetry. There are 12 bimodal coupling problems (including intra- and inter-term) in C_3 symmetry, 36 in C_{3v}, 36 in D_3, 110 in C_{3h}, 357 in D_{3h}, and 357 in D_{3d}. The seven tables hence cover 908 bimodal problems in total.

In this study, we further convert the formulas in Eqs. S9, S14, and S18 from polar to cartesian coordinates and fit them against numerically calculated matrix elements, which are obtained by running *ab initio* quantum chemistry calculations and performing diabatization on the respective grids of the cartesian coordinates that are relevant for the respective subproblems. The highest dimension in running calculations and fitting is 4 for the ${}^3E''\otimes(e'+e')$ and the ${}^3E'\otimes(e'+e')$ subproblem. The formulas up to the maximum of 6-th order are used to fit the numerical matrix elements. The order is reduced when overfitting occurs and the resultant surface is unphysical, i.e., too wavy or having wrong signs in large distortion limits. Technical details of the multi-dimensional fittings are given in Section S3 below.

It is actually more convenient to remain using the expansions in polar coordinates in fitting. One may first carry out a Fourier analysis of the numerical matrix elements. The numerical coefficients of the relevant cosine and/or sine components will then be obtained on a mesh of ρ and/or z coordinates. The coefficients are then fitted against the appropriate polynomials of the ρ and z (or ρ_α and ρ_β).

Section S3 Multi-dimensional fittings

Here, we introduce the fitting procedure to obtain the expansion coefficients for $H_{X''X''}(s_2, s_5, s_6)$, $H_{Y''Y''}(s_2, s_5, s_6)$, and $H_{X''Y''}(s_2, s_5, s_6)$. Similar procedures are used for these matrix elements expanded in other coordinates, and for the other matrix elements. We first perform electronic structure calculations in a 3-D grid of the vibrational coordinates, and extract numerical values of the matrix elements using diabatization. In scanning through the grid, the polar coordinates ρ and ϕ are used, and they are related to s_5 and s_6 as $s_5 = \rho\cos\phi$, $s_6 = \rho\sin\phi$. s_5 and s_6 are e' bending coordinates and hence have angular unit, and so does ρ. Step sizes of 10° and 15° are chosen for ρ and ϕ, respectively. One advantage of using polar coordinates is that we only need to consider the $\phi \in [0°, 60°]$ domain, which gives the symmetrically unique distortion in the s_5-s_6 space. Similarly, only the positive s_2 needs to be scanned, and we select a step size of 5°. The upper limits of ρ and s_2 are 70° and 20°, respectively. Adiabatic energies of the 4 triplet component states calculated at the upper bounds are high enough. Further distortions are unnecessary.

The calculated diagonal matrix elements are then recombined to give numerical values of $\frac{H_{X''X''}-H_{Y''Y''}}{2}$ and $\frac{H_{X''X''}+H_{Y''Y''}}{2}$. The Marquardt-Levenberg algorithm[2,3] is used to simultaneously fit the second and third expansion formulas in Eq. S9, which share the same set of expansion coefficients, against the $\frac{H_{X''X''}-H_{Y''Y''}}{2}$ and $H_{X''Y''}$ numerical values. The same algorithm is used to fit the first expansion formula in Eq. S9 against the $\frac{H_{X''X''}+H_{Y''Y''}}{2}$ numerical values. The fitted functions and the calculated numerical values of the matrix elements are plotted and compared in Figure S5, in which $s_2 = 5°$ is taken. Good agreements are seen, with all the markers falling on the surfaces, and the small deviations shown in Figure S6. The average errors of the fittings are 0.025 eV for $\frac{H_{X''X''}-H_{Y''Y''}}{2}$ and $H_{X''Y''}$, and 0.020 eV for $\frac{H_{X''X''}+H_{Y''Y''}}{2}$. Other multi-dimensional fittings give similar errors.

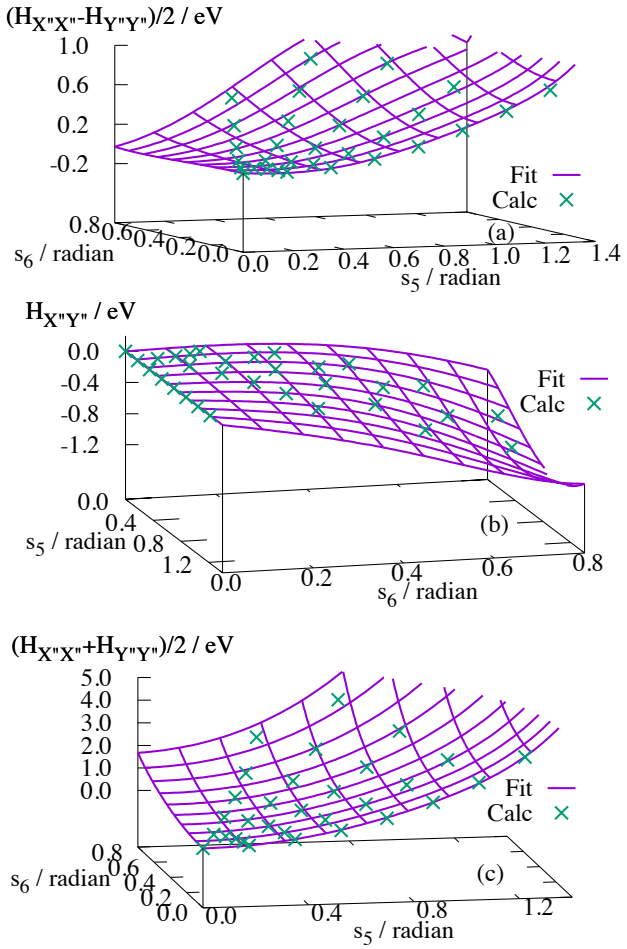

Figure S5: Calculated numerical values of (a) $\frac{H_{X''X''}-H_{Y''Y''}}{2}$, (b) $H_{X''Y''}$, and (c) $\frac{H_{X''X''}+H_{Y''Y''}}{2}$ as functions of s_5 and s_6, and their respectively fitted functions. s_2 has been set to be 5° here, and $s_1 = s_3 = s_4 = 0$.

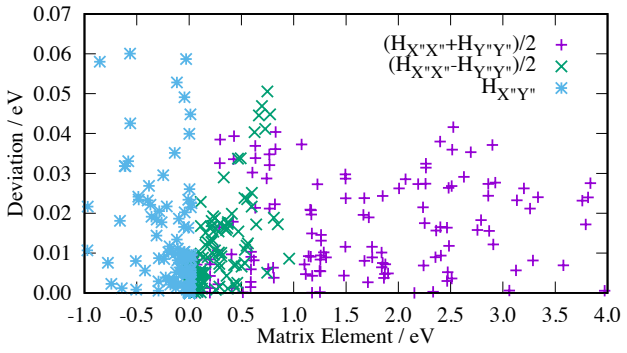

Figure S6: Deviations between the models and the numerical data in Figure S5.

Section S4 The $\underline{\underline{G}}$ matrix in constructing the $\hat{T}_N$ operator

Using the CO bond length of $r = 1.272$ Å, the $\frac{2\pi}{3}$ OCO bond angles, and the planarity of the D_{3h} reference structure, the nonzero $\underline{\underline{G}}$ matrix elements are evaluated to be

$$\begin{aligned} G^{11} = \frac{1}{m_O} = \frac{1}{15.9949 \times 1823} = 3.430 \times 10^{-5} a.u. \\ G^{22} = \frac{1}{3\mu r^2} + \frac{2}{3m_C r^2} = 9.802 \times 10^{-6} a.u. \\ G^{33} = G^{44} = \frac{1}{\mu} + \frac{1}{2m_C} = 1.029 \times 10^{-4} a.u. \\ G^{55} = G^{66} = \frac{3}{\mu r^2} + \frac{3}{2m_C r^2} = 5.3408 \times 10^{-5} a.u. \\ G^{35} = G^{46} = \frac{3\sqrt{3}}{2m_C r} = 4.941 \times 10^{-5} a.u. \end{aligned} \tag{S19}$$

$a.u.$ stands for atomic unit. μ is the reduced mass of the ^{16}O and ^{12}C nuclei.

Section S5 Technical details of the MCTDH simulations

Table S8: Technical details of the MCTDH simulations: types of DVR, ranges of coordinates in atomic units, numbers of grid points (N), and numbers of single particle functions (n).

Modes	DVR	range[a]	N	n^b
s_1	HO[c]	$[-0.3$ to $0.3]$	21	5
s_2	HO	$[-0.5$ to $0.5]$	21	7
s_3	HO	$[-0.5$ to $0.5]$	21	7
s_4	HO	$[-0.5$ to $0.5]$	21	7
s_5	HO	$[-1.0$ to $1.0]$	21	7
s_6	HO	$[-1.0$ to $1.0]$	21	7

[a] The propagated vibronic wave functions have zero amplitudes at the boundaries of these ranges. [b] A multi-set basis is used, with a common number of single particle functions in all electronic states for each mode. [c] HO stands for harmonic oscillator type of DVR.

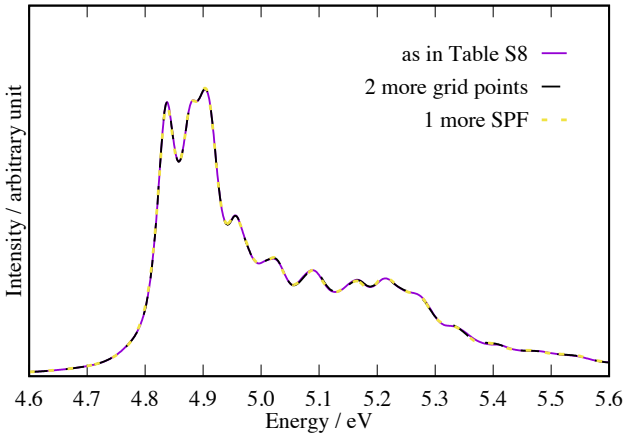

Figure S7: Convergences of simulated NIPE spectrum with respect to the numbers of grid points and SPFs.

The spectra in Figure S7 are obtained using $\mu_{E'} = 1.6\mu_{E''}$. The three spectra obtained using the numbers of grid points and single particle functions (SPFs) as in Table S8 and with two more grid points and one more SPF are indiscernible. Therefore, the simulation using the specifications in Table S8 has converged.

Section S6 The coupling between the $^3E''$ and $^3E'$ states along the s_2 coordinate.

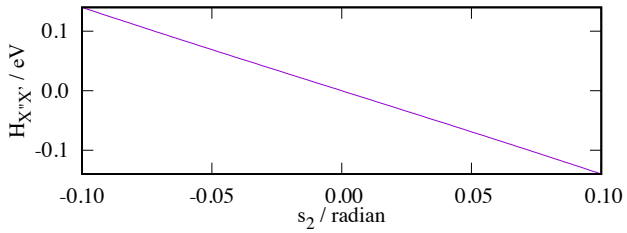

Figure S8: The coupling between the $^3E''$ and $^3E'$ states along the s_2 coordinate.

Section S7 Comparison of the simulated A band against experiment in the photon energy range of 4.8 to 5.0 eV.

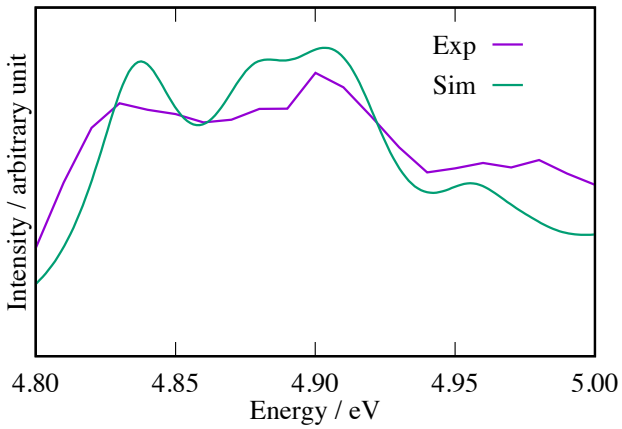

Figure S9: Comparison of the simulated A against experiment in the photon energy range of 4.8 to 4.0 eV. The simulated spectrum is obtained with $\mu_{E'} = 1.6\mu_{E''}$.

Section S8 Comparison of the simulated A band with and without the a_1' stretching.

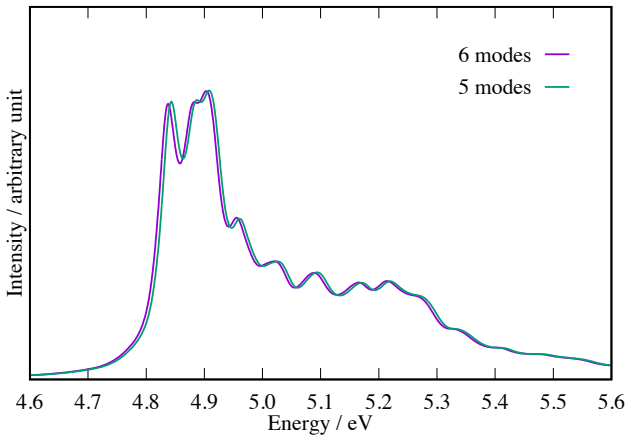

Figure S10: Comparison of the simulated A band with (6 modes) and without (5 modes) the a_1' stretching mode.

References

(1) Hickman, R. J.; Lang, R. A.; Zeng, T. *Phys. Chem. Chem. Phys.* **2018**, *20*, 12312–12322.

(2) Levenberg, K. *Quart. Appl. Math.* **1944**, *2*, 164–168.

(3) Marquardt, D. W. *SIAM J. Appl. Math.* **1963**, *11*, 431–441.